

**SELF-PROPAGATING HIGH TEMPERATURE  
REACTIONS: REMARKS AND RECENT RESULTS**

G. Cao<sup>1, 2, \*</sup>, R. Orrù<sup>1</sup>, A. Cincotti<sup>2</sup>, E. Medda<sup>1</sup>

<sup>1</sup> Dipartimento di Ingegneria Chimica e Materiali,

Centro studi sulle reazioni autopropaganti (CESRA),

Unità di Ricerca del Consorzio Interuniversitario Nazionale di Scienza e Tecnologia dei Materiali,

Unità di Ricerca del Consorzio Interuniversitario Nazionale La Chimica per l'Ambiente,

Centro Interdipartimentale di Ingegneria e Scienze Ambientali (CINSA)

Università degli Studi di Cagliari

Piazza d'Armi, 09123 Cagliari, Italy

and

<sup>2</sup> Centro di Ricerca, Sviluppo e Studi Superiori in Sardegna

VI Strada OVEST Z.I. Macchiareddu 09010 UTA (CA), Italy

\* Author to whom correspondence should be addressed

February 2000

## **Introduction**

Solid-solid and gas-solid self-propagating high temperature reactions are exploited for interesting and relatively new technological applications based on the so called Self-propagating High-temperature Synthesis (SHS) technique. As schematically shown in Figure 1, the latter one, which belongs to the more general category of Combustion Synthesis (CS), is characterized by the fact that once ignited, a relatively strong exothermic reaction is able to propagate as a combustion wave through the entire reacting mixture, without requiring any other energy supply. The main characteristics of SHS technique are its simplicity, relatively low power requirements, high combustion temperature (up to 4000 K) and front propagation velocities up to about 25 cm per second, which often permits to obtain final products with purity and mechanical properties better than those prepared by conventional methods (cf.

Merzhanov *et al.*, 1972; Munir and Anselmi-Tamburini, 1989; Varma and Lebrat, 1992; Cao and Morbidelli, 1993; Merzhanov, 1993; Hlavacek and Puszynski, 1996; Varma *et al.*, 1998). This is because, since SHS processes are characterized by very high temperature gradients (about  $10^5$  K/cm) and large reaction rates, powders of any volatile impurities adsorbed on the reactants are eliminated ("self-cleaning") during the reaction, thus leading to materials with high purity. Furthermore, the temperature gradients combined with rapid cooling may form metastable phases and unique structures not possible by conventional methods of furnace synthesis. For all these reasons, since its discovery in the early 70s (cf. Merzhanov *et al.*, 1972), SHS has received increasing attention for the synthesis of a variety of advanced materials such as ceramics, intermetallics, composites, solid solutions, functionally graded materials, etc., as shown in Table 1.

Although the many advantages mentioned above make SHS technique attractive for industrial applications, process scale-up and control is not straightforward due to the extreme processing conditions attained (cf. Hlavacek and Puszynski, 1996). In addition, combustion synthesis processes involve complex physico-chemical phenomena, such as melting and diffusion of reactants, chemical reactions with formation of intermediate phases, nucleation and grain growth, which all contribute to the formation of the microstructure of the final product. Therefore, the understanding of SHS fundamentals represents a scientific and technological challenge and, simultaneously, the key approach to develop a proper process model which can be used to address suitable control strategies. Actually, this is in general the case of reactions in condensed phases which, in spite of their technological importance, have received little attention in the chemical engineering literature (cf. Luss, 1990).

This paper reviews the recent results obtained, also in the framework of national and international collaborations, by Cao and coworkers in the field of self-propagating high-temperature reactions with particular emphasis on SHS fundamentals and applications. In particular, the research activity conducted so far can be divided into three main topics:

- Macrokinetics studies on SHS using structural statics as well as dynamics approaches.
- Modeling studies on SHS, with the aim of developing analytical expressions of combustion front velocity and simulating experimental techniques applied for macrokinetics investigations.
- Technological applications related to the synthesis of centrifugal coatings and environmental protection.

The activities outlined above will be described in this review paper in separate sections as discussed next.

### **Structural macrokinetics: static and dynamic approach.**

The main goal of macrokinetics studies is to clarify the fundamental aspects of combustion reactions occurring in condensed phases, in order to synthesize a solid product with tailored microstructure, i.e. with desired chemical and mechanical properties. This task is very difficult, since the formation of microstructure of final products obtained by combustion synthesis involves several physico-chemical steps under non-equilibrium conditions and is influenced by various processing variables (e.g., reactants particle size, green density, heating rates, initial temperature, etc.).

In order to perform macrokinetics studies different complementary approaches have been proposed in the literature. One of them, usually referred to in the literature as structural statics (cf. Mukasyan and Borovinskaya, 1992), is based on the study of the effect of processing variables (e.g., reactants particle size, green density, heating rates, initial temperature, etc.) on the final product microstructure and composition. Typically, the experimental apparatus schematically shown in Figure 2, inset a) is employed.

Although the details of the experimental set-up and procedure are reported elsewhere (cf. Cao *et al.*, 1997), temperature profiles are obtained by means of pyrometers or thermocouples embedded in the sample, while a video camera is used to monitor the propagation of the combustion wave. The final product is characterized by XRD analysis, Optical Metallography (OM), Scanning Electron Microscopy (SEM), Wavelength and Energy Dispersive Spectroscopy (WDS and EDS) microanalysis, in order to identify its chemical and microstructure composition as a function of processing variables. The recorded temperature history provides information not only, for example, about phase transitions or post combustion processes but especially the value of the maximum combustion temperature, which equals the thermodynamically calculated adiabatic temperature, in the case of negligible heat losses and complete conversion of reactants. These latter data are correlated with the measured values of combustion front velocity, in order to obtain an effective activation energy of the process using suitable analytical expressions, as discussed next.

It is apparent that the structural statics approach does not provide any elucidation of the dynamics of product formation (cf. Mukasyan and Borovinskaya, 1992).

Ideally, the mechanism of SHS reactions should be studied by using the so-called structural dynamics approach, i.e. by tracing *in situ* reactions and phase transformations. Considerable effort has been performed from the experimental point of view to highlight all physico-chemical steps and mechanisms involved in SHS reactions. Various different and complementary experimental techniques are currently available to this aim (cf. Varma *et al.*, 1998).

The most important are the following ones:

- the synchrotron radiation technique, which allows one to follow *in situ* the composition changes during front evolution, through a time-sequence of X-ray diffraction analyses;
- the particle-foil technique, which addresses the study of the interaction of few particles of one reactant with a foil of the other reactant through which current is passing in order to simulate the combustion front evolution;
- the Combustion Front Quenching (CFQ) technique, based on the rapid extinction of the reaction front during its progress, due to conductive heat losses from the sample.

Although the first technique is the only one which provides a direct observation of phase and composition changes during wave propagation, it is worth noting that the results obtained are often difficult to interpret when trying to understand the mechanism of structure formation (cf. Mukasyan and Borovinskaya, 1992). The main lack of particle-foil technique is that it does not reproduce exactly the conditions encountered in SHS reactions. On the contrary, it is recognized that the CFQ technique gives important information about the mechanism of structure formation during SHS processes (cf. Mukasyan and Borovinskaya, 1992; Quncheng *et al.*, 1996; Orrù *et al.*, 1996; Orrù *et al.*, 1998). In fact, using this

technique intermediate and final products are frozen simultaneously, and the evolution of the structure during preheating, combustion and post-combustion, may be followed by studying product microstructure and composition at different areas relatively to the location where the combustion front is extinguished.

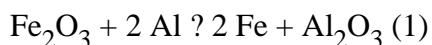
Quenching can be performed for example by dropping the reacting sample in liquid argon, placing the sample between two cooled copper plates or inside a bulk copper wedge, which can be of different shapes (cf. Cincotti *et al.*, 1999). Due to the highest cooling rate provided (cf. Mukasyan and Borovinskaya, 1992), the CFQ performed in a bulk copper wedge is preferable because is able to capture a more accurate picture of each physico-chemical phenomena involved during front evolution.

As schematically shown in Figure 3 for the case of the experimental set-up depicted in Figure 2, inset b), the starting mixture is first placed into a wedge shaped notch in a copper block and then pressed until the desired density is reached. Combustion reaction is initiated at the base of the wedge by means of a tungsten coil connected to a power supply. The combustion wave travels towards the apex of the wedge and is extinguished due to the combination of intense heat removal by the copper block and the shrinkage of the cross section.

A separate mention is needed for the Field-Activated Combustion Synthesis (FACS) technique, where the passage of an electric current through the reacting sample permits the wave propagation in relatively low exothermic reacting systems due to Joule thermal effect. In fact, some of the advanced materials listed in Table 1, i.e. most intermetallics as TiAl, do not present a relatively large exothermic enthalpy of formation necessary for the occurrence of self-propagating reactions. Moreover, volume combustion or preheating of reactants up to a temperature at which a self-propagating reaction can be initiated and sustained, often lead to final products containing secondary phases, whose undesirable presence may be a consequence of diffusion occurring during the relatively slow heating rate prior to the onset of the combustion reaction. When applying the FACS technique, the powder compact is placed between two graphite electrodes, as schematically shown in Figure 2 inset c). By simultaneously applying a sufficiently high electric field and the ignition source, a self-propagating combustion wave is initiated. Thus, structural statics experiments can be performed following the same strategy outlined above. This is also true for the case of structural dynamics investigations since the interruption of the applied field corresponds to the extinction of the combustion front (cf. Feng and Munir, 1995b; Xue and Munir, 1996a; Xue and Munir, 1996b; Gedevisanishvili and Munir, 1998; Orrù *et al.*, 1999a).

### **Structural macrokinetics: the case of thermite reactions.**

For the case of self-propagating thermite reaction, we studied the aluminothermic reduction of hematite in the presence of silica and/or alumina, as additives in order to reduce the violent character of this reaction. In fact, thermite reactions (cf. Wang *et al.*, 1993) represent a broad class of highly exothermic reactions, where a metallic or non metallic oxide is reduced by a metal to form a more stable oxide and the corresponding metal or non-metal of the reactant oxide. In the case of thermite reaction between aluminum and hematite, the product consist of a heavier metallic phase and an oxide phase as indicated by:



This type of reaction is exploited in a variety of technological applications such as the synthesis of refractory ceramic and composite materials (cf. Merzhanov, 1990 and reference therein) and the

preparation of ceramic linings in metallic pipes (cf. Odawara, 1990; Yin *et al.*, 1993; Chandran *et al.*, 1995; Orrù *et al.*, 1995). In fact, the obtained phases can be conveniently separated by gravity when the molten state is reached, as it will be illustrated later in the SHS technological applications section.

Numerous experimental studies had focused their attention to determine the factors affecting the combustion rate of thermite reactions including particle size of reactants, addition of inert diluents, pre-combustion compact density, salt addition, centrifugal force, ambient inert gas pressure and the physical and chemical stability of oxide reactants (cf. Wang *et al.*, 1993). On the contrary, only little information regarding the formation of the microstructure of products obtained by thermite reactions was available in literature. This basic knowledge not only represents the most important factor which determines the properties of materials (strength, stability, ductility, etc.) but also may be considered as a reference study when investigating the mechanism of structural transformations of thermite reactions.

We then performed structural statics investigations on the microstructure of the product of the self-propagating thermite reaction between aluminum and hematite by varying the alumina or silica content in the starting mixture (cf. Orrù *et al.*, 1997) due to their utilization for the preparation of ceramic linings in metallic pipes (cf. Odawara, 1990; Yin *et al.*, 1993; Chandran *et al.*, 1995; Orrù *et al.*, 1995). The details of the experimental set-up schematically shown in Figure 2 and the applied procedure are reported elsewhere (cf. Orrù *et al.*, 1997). Basically, the green mixture, constituted of reactants in stoichiometric ratio according to Equation (1) and different weight percentage of additives (7, 18 and 25% or 7, 12, 15, 25%, for alumina or silica, respectively), was pressed into cylindrical pellets (densities range from 2.2 to 2.3 g/cm<sup>3</sup> and 2.2 to 2.5 g/cm<sup>3</sup> depending upon the alumina and silica content, respectively), and ignited at its base by means of a tungsten coil connected to the power supply depicted in Figure 2.

As indicated by the videotapes, the melting processes involved are more pronounced when decreasing the percentages of either alumina and silica in the starting mixture. Although the increase of alumina content affects the reaction conditions, as revealed by the decreasing of the maximum values of the measured combustion temperatures reported in Table 2, the detected crystalline phases are always corundum (Al<sub>2</sub>O<sub>3</sub>), hercynite (FeO·Al<sub>2</sub>O<sub>3</sub>) and iron.

The situation substantially changes when adding silica to the starting mixture. Mullite (3Al<sub>2</sub>O<sub>3</sub>·2SiO<sub>2</sub>) and iron are always revealed regardless the silica content. In particular, these are the only reaction products in crystalline form at 25% of silica. However, as its content decreases, hercynite is found for values of silica equal or lower than 15%, while corundum is detected only at or below 12%. Also in this case the maximum temperature measured during the course of the reaction decreases by increasing the silica content, as it may be seen in Table 3.

After etching with a dilute solution of hydrochloric acid, the microstructure of the reacted pellet with 25 wt% of alumina may be seen in the SEM back-scattered micrograph shown in Figure 4. Iron (a), corundum (b) and hercynite (c) are then identified by WDS. Except for the crystal and pore sizes, no variations in the microstructure of the pellets reacted with the other values of alumina content are detected. The microstructure of the reacted pellets with different silica content has been investigated (cf. Orrù *et al.*, 1995) but the corresponding results are not reported here for sake of brevity.

Next, by means of the CFQ technique, we investigated the mechanism of the self-propagating thermite reaction between aluminum and hematite with alumina added to the starting mixture (cf. Orrù *et al.*, 1996; Orrù *et al.*, 1998). Two starting mixtures containing 25% wt of additives were prepared and then

pressed (green density equal to 2.67, and 2.29 g/cm<sup>3</sup>, when adding alumina or silica, respectively) inside a cylindrical copper block, with a wedge shaped notch as depicted in Figure 2, inset b). Experimental set-up and procedure are reported elsewhere (Orrù *et al.*, 1996) for sake of brevity.

A SEM back-scattered image of the sample where the combustion front is extinguished allows us to distinguish the presence of four zones, as shown in Figure 5. As moving upwards from the unreacted region (1), the light phase (2) gradually vanishes thus encountering a single-phase region (3). Region (2) is constituted by aluminum (m) and alumina (n) particles and iron oxides (p), as revealed by WDS microanalysis. These are magnetite and wustite as confirmed by XRD analysis. Aluminum and alumina particles are surrounded by different iron-aluminates (q). These may be considered as the result of the first interaction between the species involved in the aluminothermic reaction. This interaction increases giving rise to amorphous iron-aluminates (3), where all the alumina of the system is present. In the same region grains of iron and hercynite start to appear. However, these species are present in larger amounts in the heterogeneous region (4). Alumina is present as corundum (x), whose grains grow up to about 10 µm as the distance from the zone (3) increases, being hercynite (y) distributed at the boundary. Iron spots (w) appear to be dispersed in region (4). It is worth noting that final products revealed in the latter region correspond to those obtained by reacting the same starting mixture without quenching conditions (cf. Orrù *et al.*, 1997).

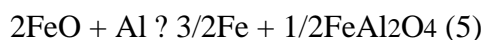
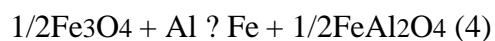
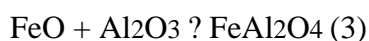
More complex and interesting results obtained for the case of silica as additive in the starting mixture are not considered here for sake of brevity (cf. Orrù *et al.*, 1996).

By coupling the information obtained from the various analytical techniques employed as described above together with the study of the interaction of ferric oxide particle on aluminum film using high-temperature diffraction electron microscopy (cf. Korchagin and Podergin, 1979), the following considerations can be made (for the case when alumina is added to the starting mixture).

The formation of magnetite can be explained on the basis of the thermal decomposition of hematite:



while FeO may result from the subsequent thermal decomposition of magnetite. The formation of hercynite and the simultaneous presence of iron detected moving towards region (z) of Figure 10 may be due to the occurrence of the following reactions:



Iron-aluminates in amorphous form, detected in region (z) of Figure 5 may be viewed as intermediate products of the reaction process, which have been "frozen" due to the high quenching rate provided by the copper block in a very short time. Final products detected in region (4) of Figure 5, i.e. corundum and hercynite, appear then to be formed through a crystallization process from the melt corresponding to the amorphous region (z). From the FeO - Al<sub>2</sub>O<sub>3</sub> phase diagram (cf. Fischer, 1956), due to the high alumina content in the melt (atomic ratio aluminum / iron equal to about 4.94 as obtained from WDS), alumina crystallizes first because of its higher solidification temperature with respect to hercynite. Then,

the crystallization of the eutectic hercynite-corundum takes place. It should be noted that primary alumina undergoes also a continuous grain size increasing, as it may be seen moving upwards in Figure 5 due to more favourable grain grow conditions encountered. The formation of iron may be explained on the basis of equation (4) and (5). The results above may be schematically represented in Table 4 where the structure formation zones, which should be passed in order to convert reactants into products, are summarized.

With the aim of better elucidating the reaction path of the aluminothermic reduction of hematite in the presence of alumina, we compared the results obtained under SHS conditions, either with or without CFQ, with those resulting from the use of Ball Milling (BM) technique. This goal is accomplished by characterizing in details intermediate phases and final products by means of an extensive use of X-ray diffraction and Mössbauer spectroscopy, together with microstructure observations. Although the results obtained are not reported here (the interested reader should refer to Cao *et al.*, 1997), it should be noted that BM offers the possibility of controlling the evolution of reaction so that its path can be studied by properly choosing the process parameters (i.e. milling mechanics, diameter of balls, ball to powder weight ratio).

In particular, we found a similar reaction path in SHS and BM reaction under argon atmosphere, even if the two reaction techniques are quite different. However, SHS reaction involves also the formation of a melt from which the product crystallize, while BM proceeds through solid state reactions and no melting takes place.

### **Structural macrokinetics: the case of titanium aluminides.**

Let us now consider the case of titanium aluminides  $Ti_3Al$  and  $TiAl$ , for which the feasibility of synthesizing through FACS was demonstrated for the first time by Orrù *et al.*, 1999a.

The potential use of titanium aluminides in structural and aeronautical applications have generated considerable interest in these materials in the past decade. These intermetallics possess a combination of physical and mechanical properties which make them attractive for these and other applications. The desired properties include low density, high specific strength, excellent creep resistance, and high temperature oxidation and corrosion resistance (cf. Froes *et al.*, 1992). However, this class of materials is characterized by room temperature brittleness, and some of the current research is aimed at improving their ductility through various approaches, including the use of new methods of production, or through alloying.

Several methods have been utilized in the synthesis of Ti-Al intermetallic compounds. These include conventional melting and casting processes and powder metallurgical techniques (cf. Froes *et al.*, 1992). The latter include mechanical alloying (cf. Suryanarayana *et al.*, 1997), plasma rotating electrode processes, and inert gas atomization (which have been recently proposed as methods of preparing titanium aluminides in powder form). In all of these approaches, a subsequent step is required to obtain products with the desired density and shape.

Here, we report the results of the synthesis of  $Ti_3Al$  by means of FACS technique, which has been applied for the synthesis of a variety of materials with low adiabatic temperature values (cf. Feng and Munir, 1994, 1995b; Gedevisishvili and Munir, 1995; Munir, 1997).

Powders of titanium and aluminum were mixed in stoichiometric ratios corresponding to the compound

Ti<sub>3</sub>Al, and pressed with resulting relative green density in the range of 55-75%, depending on the applied pressure. Details of starting mixture preparation and experimental procedures are reported elsewhere (cf. Orrù *et al.*, 1999a). Briefly, pellets were placed between two graphite electrodes across which a voltage was imposed simultaneously with the ignition source, as schematically shown in Figure 2, inset c). The ignition source was turned off immediately after the reaction was initiated and the wave began to propagate. The influence of the applied electric field and the effect of green density were examined through a video recorder and a two-color pyrometer to determine wave velocity, while XRD analysis was adopted to characterize the reaction products.

Wave initiation and propagation required a threshold value of the imposed electric field, as clearly shown in Figure 6. The dynamics of the combustion wave, i.e. front velocity and combustion temperature profiles, were dependent on field strength. The concept of a threshold, i.e. the need for activation, relates to the requirements of energy for the combustion wave propagation in relatively low exothermic reactions, such the synthesis of titanium aluminides. From previous experimental observations and modeling studies (cf. Feng and Munir, 1994, 1995a, 1995b; Munir, 1997), it was concluded that the role of the field is to provide additional energy in the form of Joule heat to the reaction wave, and then depends on the electrical conductivity of the system and the applied electric field.

Although a wave can propagate above the threshold values, using low field levels the reactions were not complete and the product was multiphase, containing four titanium aluminides and unreacted titanium, as can be seen in XRD patterns reported Figure 7. The amount of secondary phases in the final products decreased with increasing field strength, and a single phase product can be obtained at high fields. This dependence of the nature of the product (and by implication the mechanism of the synthesis) on the magnitude of the applied field was the most significant observation of our investigations. That the field can influence the mechanism of synthesis has been previously demonstrated in the case of tungsten silicides (cf. Gedevanishvili and Munir, 1995). However, in that case the change in the nature of the product occurred over a very narrow field range unlike the present case where the relative concentration of the desired phase increased gradually with increased field. The importance of the present results is that the application of a field can be considered as a processing parameter during FACS synthesis.

A unique effect of reactant compact density was also found. Specifically, wave velocity, combustion temperature, and product purity increased as the relative density decreased, as can be seen in Figures 8 and 9. These results suggest that an optimization of the synthesis of Ti<sub>3</sub>Al can be achieved through an appropriate combination of the processing parameters of initial density and applied field.

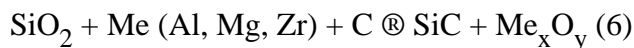
Next, the reaction mechanism of the FACS of the phase Ti<sub>3</sub>Al from elemental powders (relative density = 55%) was investigated, by turning off the applied field ( $E = 14.3$  V/cm) during wave propagation so that combustion front ceased to advance immediately (cf. Orrù *et al.*, 1999b). Figure 10 shows a longitudinal cross-section of the quenched sample. A layer to layer X-ray diffraction analysis performed at various axial locations (i.e., parallel to wave propagation) of the quenched sample made possible the identification of four regions. Their positions are schematically represented in Figure 10, together with the corresponding XRD patterns. Region 1, ahead of the wave, is made up of the elemental reactants only. Region 2 contained TiAl<sub>3</sub> together with unreacted titanium and aluminum. The latter was not detected in Region 3 where TiAl was found together with the desired phase Ti<sub>3</sub>Al and unreacted titanium. Finally, in Region 4 only the desired phase Ti<sub>3</sub>Al was detected.



By coupling XRD analysis above with a detailed microstructure investigation, not reported here for sake of brevity, it was postulated that the combustion reaction was preceded by the melting of aluminum which then spreads over the titanium particles. Liquid aluminum then reacts with the titanium particles giving rise to a layer of  $\text{TiAl}_3$ . Subsequently, the unreacted Ti reacts with  $\text{TiAl}_3$ . This leads to the formation of Ti cores surrounded by a layer of  $\text{Ti}_3\text{Al}$  which is followed by a layer of TiAl. This interaction continues leading to the shrinkage of the Ti cores, the gradual disappearance of the TiAl layer, and the simultaneous increase of the  $\text{Ti}_3\text{Al}$  content. A single  $\text{Ti}_3\text{Al}$  phase product was finally formed. The proposed mechanism is summarized in Table 5.

### **Structural macrokinetics: the case of $\text{ZrO}_2/\text{SiC}$ composite containing SiC whiskers.**

Ceramic materials constituted by  $\text{SiC}/\text{Me}_x\text{O}_y$  and reinforced with SiC whiskers have wide application in different new and emerging areas (cf. Tennery, 1989; Hunt, 1990) because of their high operating performances (high hardness, durability, cracking resistance, etc.). The synthesis of powders of the above-stated compositions under the SHS mode, may be conducted through the following schematic reducing stage:



which, however, is not self-sustaining due to the solid-phase mechanism of the combustion reaction, the presence of protective oxide films on metals, etc. (Nersisyan *et al.*, 1999). On the other hand, the self-propagating combustion process may be activate by introducing into the initial mixture a small amount of functionally active compounds, so called combustion promoters (mainly, halogen containing organic polymers, nitrates of alkaline metals, etc.). While the details of the experimental procedure are reported elsewhere (cf. Kostanyan *et al.*, 1999), it should be noted that zirconium powders with particle size range of 2-15  $\mu\text{m}$ , carbon black granulated with particle size less than 1  $\mu\text{m}$  and  $\text{SiO}_2$  were used to prepare the starting mixtures. As a promoter of combustion reaction powdered teflon -  $(\text{C}_2\text{F}_4)_n$  with particle size less than 10  $\mu\text{m}$  was employed. The promoter content in the initial mixture varies in the range of 0.1-5.0 wt.%. As carbon-containing gas-generating additives, powdered hydrocarbon polymers, such as polystyrene -  $(\text{C}_8\text{H}_8)_n$ , polyethylene -  $(\text{C}_2\text{H}_4)_n$ , polypropylene -  $(\text{C}_3\text{H}_6)_n$  with particle size range of 1-10  $\mu\text{m}$ , were used. Pellets, prepared following standard procedures, were reacted using the apparatus depicted in Figure 2, inset a).

Microstructure investigation of reaction products obtained from initial mixtures of the system  $\text{SiO}_2/\text{Zr}/\text{C}/m(\text{C}_2\text{F}_4)_n$  (where  $m=0,3-5,0$  wt.%) have shown that the end-products display a characteristic morphology (cf. Nersisyan and Kharatyan, 1995; Nersisyan *et al.*, 1999).

It was established that the activation of combustion process takes place by means of gaseous zirconium fluorides formed at the initial stage of the process which interact then with  $\text{SiO}_2$  particles and the intensive formation of SiC whiskers occurred mainly in free volumes (pores).

With the purpose of increasing the SiC whiskers formation in the reaction products, the amount of carbon in the initial mixture was replaced by hydrocarbon polymers, in particular polystyrene, polyethylene and polypropylene. Such replacement was justified since hydrocarbon polymers, being

decomposed during the combustion process, create high density of carbon-containing gases in sample pores where whiskers are formed.

According to microstructural analysis data, with increasing of polystyrene content in the starting mixture the amount of SiC whiskers in end-products sharply increases. The micrographs of the microstructure of the fracture of burned down samples with different polystyrene content are shown in Figures 11a-11b. It is seen from Figure 11a that substitution of 10 wt.% carbon by polystyrene results in noticeable amount of SiC whiskers. The whiskers thickness is about 0.1-0.5  $\mu\text{m}$ , length up to hundred microns. The distribution of whiskers in reacted sample is more uniform in comparison with the case when no polystyrene is added. If polystyrene amount is increased up to 30 wt.% a thin fluffy layer of SiC results to cover all the exterior surface of sample, as it may be seen from Figure 11b. Spherical particles are also found at the end of the whiskers. Probably, these particles were originally drops of silicon, from which the whiskers grew. Because of high concentration of carbon in gas medium these drops react rapidly and, under certain conditions, turn into silicon carbide, thus retaining the spherical shape. At specific locations of the burned down samples the whiskers display a precise orientation. The orientation of whiskers coincides with streamline of gaseous products leaving the reaction zone.

Since, as discussed elsewhere (cf. Nersisyan and Kharatyan, 1995; Nersisyan *et al.*, 1999), the whisker formation takes place from gaseous phase, it is interesting to investigate the influence of pressure and composition of gaseous medium on combustion patterns and whiskers growth. The experiments were carried out with an initial composition  $\text{SiO}_2/\text{Zr}/\text{C}/4\%(\text{C}_2\text{F}_4)_n/10\%(\text{C}_8\text{H}_8)_n$ , under nitrogen and argon atmosphere. As it follows from Figure 12, the combustion parameters ( $T_c$ ,  $U_c$ ) increase with increasing pressure and thus reaching at certain values of  $P_{\text{N}_2}$  ( $P_{\text{N}_2} > 2,5 \text{ MPa}$ ) a plateau. It is possible to explain this behaviour since an increase of pressure is able to avoid the heat ablation processes from reaction zone due to the expelled gases. In Figure 12 the values of  $T_c$  and  $U_c$  for samples burning in argon medium are also reported. Differences in  $T_c$  values are small and remain in the range 20-100 K.

Microstructural analysis indicates that as pressure increases SiC whiskers become shorter and lose orientation. This behavior may be related to the fact that processes related to gas emissions within the reacting system, which have a favorable effect on growth and orientation of whiskers, are suppressed. At high nitrogen pressures compact fine-grained clusters of  $\text{ZrO}_2$  are frequently encountered in end-products, as it may be seen Figure 13. At larger magnifications, these particles become similar to crystals with defined facets of tetragonal shape. Taking into account the significant increase of combustion temperature at high pressures one can assume that these crystals were formed from  $\text{SiO}_2$ -Zr melt.

As substances promoting intensive formation and growth of SiC whiskers besides polystyrene, powdered polyethylene and polypropylene were also tested. It was shown that these polymers act similarly to polystyrene. Thus, it was concluded that the introduction of hydrocarbon polymers into the initial mixture favours an intensive growth of SiC whiskers and the occurrence of gas-transport mechanism of zirconium transfer results in fine structures of end-products.

### **Self-propagating high-temperature reactions modeling: analytical solution for solid-solid systems.**

Although self-propagating high-temperature reactions take place in heterogeneous media, as clearly seen from the reacting systems described above, modeling approach typically adopted is based on the theory

of combustion which neglects mass transfer by diffusion at microscopic level. Thus, by considering homogeneous systems, the following mass and energy balance equations may be written:

$$\square \quad (7)$$

$$\square \quad (8)$$

where  $h$  is the conversion of the limiting reactant,  $T$  is the temperature while the significance of other symbols is reported in the Nomenclature.

In general, in order to identify the reaction rate expressions  $\square$ , the reacting mixture is either treated as homogeneous or, when the heterogeneous nature of the system is accounted for, the rate function used is not related directly to a physical description of the reaction process. The general form of the reaction rate may be written as (cf. Varma and Lebrat, 1992):

$$\square \quad (9)$$

where  $\square$  varies with the system chemistry and geometry. For the case of homogeneous combustion,  $\square$  may be represented by an  $n$ -th order function:

$$\square \quad (10)$$

while if the reaction is assumed to occur as a result of diffusion of one reactant through the layer of a forming solid product (i.e. the heterogeneous nature of the process is accounted for), we have:

$$\square \quad (11)$$

where  $m$  and  $n$  are usually determined empirically.

While Equations (7) and (8) have been solved numerically in the literature by several authors (cf. Varma *et al.*, 1998) to quantitatively describe various reacting systems, here we report the strategy to obtain analytical solutions of the same Equations for the case of solid-solid and gas-solid systems.

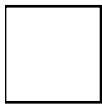
In fact, the development of theoretical formulas which correlate the combustion parameters, i.e. combustion temperature, speed of propagation, and the kinetic parameters, i.e. activation energy, in order to estimate the latter ones from experimental data, has received considerable attention in the literature (cf. Merzhanov and Khaikin, 1988; Munir and Anselmi Tamburini, 1989; Varma and Lebrat, 1992; Merzhanov, 1993).

In particular, since the pioneering work of Novozhilov (1961), several expressions for the velocity of the combustion front have been obtained (cf. Merzhanov, 1977) depending upon both the elementary combustion model and the reaction rate function utilized.

Using a reaction rate function related directly to a physical description of the reaction process, a new analytical expression for the velocity of the combustion front was developed (cf. Cao and Varma, 1994; Cao and Varma, 1995) for the case of a solid-solid reacting system, which in general can be represented according to the scheme:

(12)

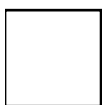
where A and B are the low-melting-point and nonmelting components, respectively, while P is the reaction product used also as inert diluent. Based on experimental observations of several systems (including Fe<sub>2</sub>O<sub>3</sub>-Al, Ni-Al, Ti-C, Nb-C, Ta-C, Ti-B, Nb-B, Ta-B, Hf-B), Aleksandrov and Korchagin (1988), postulated a mechanism for the SHS reaction between two solid reactants, which assumes that the reaction rate is proportional to the instantaneous surface area of nonmelting component and to the instantaneous concentration of the melting reactant in the formed outlying melt. By taking these considerations into account, Kanury (1992) developed an instantaneous reaction rate expression from first principles of mass and species conservation. By considering the schematic representation of the reaction process as depicted in Figure 14, the rate expression may be written in terms of molar consumption of the non-melting component as follows:



(13)

where D represents the ratio between the particle diameter of the nonmelting component at time t (i.e.  $d_p$ ) and the corresponding value at  $t = 0$  (i.e.  $d_{p0}$ ).

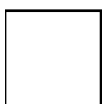
The expression of the concentration of the melting component (A) in the melt surrounding the nonmelting particle (B),  $C_{am}$  is given by:



(14)

where the meanings of all other symbols are reported in the Nomenclature. It is worth noting that the rate of reaction given by Equation (13) accounts for the influence of temperature, particle size, reactant consumption and inert dilution.

In order to find an analytical expression for the front propagation velocity from Equations (7) and (8), it is necessary to relate the instantaneous reaction rate of Equation 7 to the ratio D of Equation 13. For the case when the initial mixture is rich in the melting component (A), the extent of conversion of the nonmelting reactant particle can be defined as:



(15)

where  $a$  represents the moles of melting reactant (A) per mole of nonmelting reactant (B) in the initial mixture, according to the reaction scheme reported in Equation (12). On the other hand, if the initial mixture is deficient in the melting component (A), the extent of conversion can still be defined in terms of the nonmelting reactant particle as:

$$\square$$

(16)

It is apparent that in both cases, the extent of conversion  $h$  varies from zero to unity. For  $a > 1$ , the nonmelting reactant (B) gets fully reacted when  $h = 1$ ; on the other hand, for  $a < 1$ , the melting reactant (A) is fully consumed when  $h = 1$ . Depending upon the value of  $a$ , by coupling Equations (13) and (14), the following rate of reaction can be obtained:

(17)

Thus, for the case of an adiabatic cylindrical pellet of infinite length where all the physical properties are assumed to remain constant, Equations (17), which represent the relevant mass balance, needs to be coupled with the one-dimensional energy balance given by Equation 8, along with the following initial and boundary conditions:

$$\square$$

(18)

$$\square$$

(19)

$$\square$$

(20)

It is worth noting that we have chosen a pellet of infinite length under adiabatic conditions in order to analytically derive an expression for the velocity of the combustion front. Regarding the choice of infinite length, it has been shown recently (Cao *et al.*, 1991; Varma *et al.*, 1992) that although the combustion front does not move with constant velocity in pellets of finite length, the velocity in case of the latter is essentially constant for much of the reaction, except for end effects. Since this constant value corresponds to that for infinitely long pellets, it is apparent that the results obtained for infinitely long systems are also applicable to finite pellets.

Assuming that the combustion front propagates at a constant velocity ( $v_f$ ), i.e. constant-pattern behavior prevails, an eigenvalue problem may be obtained from Equations 7-8 and 18-20 (cf. Merzhanov, 1977; Puszynski *et al.*, 1987). Introducing the so-called *thin-zone* assumption, which implies that the reaction

is confined to a relatively narrow zone near the propagating front, the following expression for the front propagation velocity can be derived:

$$\square \quad (21)$$

where

$$\square \quad (22)$$

and depending on the value of  $a$ , the forms of the integral  $I_2$  are given by:

$$\square \quad (23)$$

$$\square \quad (24)$$

Next, by applying the well-known Frank-Kamenetskii approximation, the integral appearing in Equation (21) can be approximated as follows:

$$\square \quad (25)$$

Equations (21), (22) and (23) [or (24)] provide the approximate analytical expression for the velocity of the combustion front, for the case of an SHS process occurring in an infinitely long pellet consisting of spherical particles, reacting according to the mechanism discussed above, which simultaneously accounts for the influence of temperature, particle size, reactant proportions and inert dilution.

By considering the parameter values reported in Table 6, a comparison between analytical and experimental results for the velocity of propagation front as a function of dilution with inert product,  $q$  is

presented in Figure 15. This quantity is related to the moles of diluent (TiC) per mole of carbon in the initial mixture,  $b$  as follows:

$$\square \quad (26)$$

A good agreement with the experimental data is found. When comparing the analytical results with the numerical values obtained by Huque and Kanury (1993), it is seen that for small dilution with product the analytical results lie above the numerical ones, as observed before. However, for increased dilution, a crossover between the two curves is found which is difficult to explain.

### Self-propagating high-temperature reactions modeling: analytical solution for gas-solid systems.

The case of gas-solid reactions has been deeply investigated from the theoretical point of view by Aldushin and coworkers (cf. Aldushin *et al.*, 1974, 1980; Aleksandrov and Korchagin, 1988), who developed the theory of filtration combustion, in which self-propagating reactions are found to occur under two limiting cases, i.e. the so-called filtration and kinetic mode, depending upon the availability of the fluid reactant in the reaction zone. Several interesting results which contribute in the direction of the understanding of the involved phenomena were obtained (cf. Aldushin *et al.*, 1974; Aleksandrov and Korchagin, 1988), while the rate functions used have invariably an empirical character. Agrafiotis *et al.* (1991), interpreted the gas-solid SHS reaction between tantalum and nitrogen by means of the sharp-interface model (SIM), based on a  $n$ -th order irreversible reaction taking place at the interface between the exhausted outer shell of the product and the unreacted core of the metal (cf. Dorayswamy and Sharma, 1984), assuming negligible filtration resistance. However no explicit relationships for the velocity of the combustion front were reported.

Assuming no filtration limitations, a new analytical expressions for the velocity of propagation front for the case of an infinitely long system was developed (cf. Orrù and Cao, 1996), by incorporating the SIM into a one-dimensional model of SHS reaction between a gas, A and spherical particles of radius  $R_0$  of solid, B, according to the following general scheme:

$$\square \quad (27)$$

The reaction is supposed to occur at a sharp interface between the exhausted outer shell and the unreacted core of the solid, i.e. the SIM holds. By assuming constant particle size, and defining the extent of conversion of the solid particle as:

$$\square \quad (28)$$

the rate of reaction expressed as  $\square$  is reported in Table 7, depending upon the possible controlling regimes:

- external diffusion;

- internal diffusion with the following exponential dependence of the effective diffusivity on temperature (cf. Aldushin *et al.*, 1980):

$$\square \quad (29)$$

- kinetic regime, with the following power law expression:

$$\square \quad (30)$$

or the Langmuir-Hinshelwood (L-H) one:

$$\square \quad (31)$$

- no controlling regime and reaction order equal to one at the reaction interface.

To derive an analytical expression for front velocity, the same mathematical procedure described for solid-solid systems is taken into account. Thus, in order to describe the SHS process occurring in a adiabatic infinite long cross-flow reactor (cf. Orrù and Cao, 1996), where all physical properties of the solid and gas remain constant, the concentration gradient of gas along the bed length and depth is negligible, the relevant mass balance needs to be coupled with the one-dimensional energy balance given by Equation (8), along with the following initial and boundary conditions:

$$\begin{array}{|c|} \hline \square \\ \hline \square \\ \hline \end{array} \quad (32)$$

$$(33)$$

$$\square \quad (34)$$

where  $\square$  is generally assumed to be equal to the combustion temperature.

Assuming that the combustion front propagates at a constant velocity ( $v_f$ ), i.e. constant-pattern behavior prevails, an eigenvalue problem is obtained also in this case. By introducing the so-called *thin-zone* assumption, which implies that the reaction is confined to a relatively narrow zone near the propagating front, the expressions for velocity of the combustion front reported in Table 8 may be obtained. It should



be noted that the integral involving the exponential dependence of the temperature was solved by applying the already mentioned Frank-Kamenetskii approximation:

$$\square$$

(35)

where E is either  $E_K$  or  $E_D$ . The solution for the external diffusion regime is not shown in Table 8, since it has never been considered under SHS conditions. This also means that for the last case of Table 7,  $Bi \gg 1$ .

Note that for an analytical solution of regimes 4 and 5 in Table 7, two further assumptions are required: negligible temperature dependence of the adsorption equilibrium constant ( $K_A$ ) and  $E_K = E_D$ .

It should be noted that the expressions reported in Table 8 account for the influence of combustion temperature, gas pressure, particle size, reactant properties and inert content. The dependence of the gas pressure is represented by the bulk gas concentration,  $C_{Ab}$  which may be expressed through the ideal gas

law, i.e.  $\square$ .

A comparison between theoretical predictions of this analytical expression for the velocity of the combustion front and suitable experimental data of Agrafiotis *et al.* (1991) for the system nitrogen/tantalum is reported next. In particular, for the case of the kinetic regime, a linear fitting of

$\square$  versus  $\square$  data displays a slope proportional to the activation energy and an intercept which is a function of  $k_{i0}$  and  $n$  (power law kinetics) or  $k_{i0}$  and  $K_A$  (L-H law kinetics).

As shown in Figure 16, using the values of the parameters reported in Table 9, a straight line is obtained, whose slope allows us to evaluate an activation energy of about 150 kJ/mol which compared fairly well not only, as expected, with the value calculated in Agrafiotis *et al.* (1991), but also with the one evaluated by other authors (cf. Hirao *et al.*, 1988) for the same system.

From intercepts values of Arrhenius-like plots mentioned above, the remaining unknown kinetic parameters were evaluated by fixing  $n$  and obtaining  $k_{i0}$  or fixing the ratio  $k_{i0}/K_A$  and obtaining  $k_{i0}$  and  $K_A$ . It was found (cf. Orrù and Cao, 1996) that depending upon the combination of the parameters a good comparison with the experimental data is found. In particular, the values of  $n = 0.25$  and  $k_{i0} = 0.82$

$\square$ , and  $k_{i0} = 1.38 \square$  and  $k_{i0}/K_A = 1.5 \square$  are responsible for the best agreement with the experimental data for the case of the power law and L-H kinetics, respectively. It should be noted that, while the comparison with the experimental data obtained at 55 atm is the result of a fitting procedure, the values of the front velocity at the other pressure levels should be regarded as predicted by the velocity expressions derived. Therefore the experimental behavior of the velocity dependence on the nitrogen pressure may be also interpreted on the basis of non-linear kinetics without invoking filtration limitations.

**Self-propagating high-temperature reactions modeling: numerical simulation of the copper block**

### CFQ technique.

Although the CFQ technique in a bulk copper wedge is able to provide detailed information of macrokinetic type useful for process understanding as shown earlier, the evaluation of the physico-chemical parameters involved may be obtained only by direct comparison between experimental and theoretical results. When following this standard and efficient approach by adopting the CFQ technique, since heat transfer phenomena cannot be uncoupled from the other physico-chemical ones (diffusion of reactants, nucleation and grain growth, etc.), it is necessary to develop a mathematical model of this technique able to provide a reliable tool for parameters estimation.

However, to our best knowledge, the only work available in the literature addressing the modeling of the copper block CFQ technique (cf. Stepanov and Rogachev, 1992) provides theoretical results which are not consistent with experimental evidence, due to an inadequate description of the heat transfer phenomena.

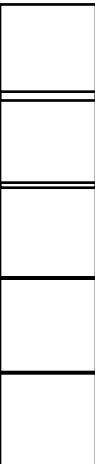
With the aim of contributing towards the development of a more reliable simulation of the copper block CFQ technique, a two dimensional model of a SHS reacting system placed inside a wedge-shaped cut in a copper block which incorporates a detailed description of the heat transfer phenomena was developed (cf. Cincotti *et al.*, 1999).

Assuming a pseudo-homogeneous behavior of the reacting system with constant physical properties and a first-order power law kinetic, i.e.  $n = 1$  in Equation 10, the mathematical model of the CFQ technique based on a wedge-shaped cut in a copper block (CFQCW in the sequel), is constituted by mass and energy balances for the reacting mixture, i.e. Equations (7) and (8), expressed in cylindrical coordinates, and by the following energy balance


$$(36)$$

for the copper block. In Figure 17 a sketch of the system adopted for modeling purposes is reported.

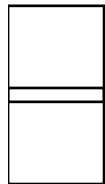
The initial and boundary conditions to be coupled to the equations (7), (8) and (36) are as follows:


$$(37)$$
$$(38)$$
$$(39)$$
$$(40)$$
$$(41)$$

Note that Equation (38) represents the cylindrical symmetry condition, while Equation (40) reflects the

null heat flux due to the insulating wooden support upon which the copper block is placed as shown in Figure 17. Radiative and newtonian heat fluxes from external copper block wall to air are considered in Equation (39). In Equation (41), the normal components of the conductive heat fluxes at the reacting sample-copper block interface are considered to be equal. The boundary condition at  $z = 0$  can be expressed as follows:

Unfortunately, an accurate value of the flux  $p$  is available in the literature only when a laser is used as ignition source (cf. Dimitriou *et al.*, 1989). Since, on the other hand, the simulation of the heat flux provided by the tungsten coil used experimentally is very complex, the following boundary condition was adopted:



(43)

where  $g(t)$  is an empirical function obtained by interpolating the experimentally determined temperature profiles corresponding to three different radii at the base of a reacting sample, as shown in Figure 18. In particular, the graphite and titanium system, mixed in stoichiometric ratio according to reaction  $Ti + C \rightarrow TiC$  with 20 % by weight of titanium carbide as diluent, has been considered.

Details of the experimental set up and procedure related to this work are reported elsewhere (cf. Cincotti *et al.*, 1999), for sake of brevity.

The equations corresponding to the system CFQCW are solved numerically discretizing the spatial derivatives at the internal node points in the  $z$  and  $r$  directions, and integrating the resulting system of ordinary differential equations by means of DIVPAG-IMSL standard routines. Since a uniform mesh of about  $555 \times 377$  discretization points was generally kept, a high performance multi-processor computer (CRAY T3E DEC Alpha 21164, 600 Mhz) was used in order to reduce the computational time. Higher values of the internal node points did not cause any change in the results.

The model parameters reported in Table 10 which are related to the reacting mixture as well as the specific copper block configuration adopted experimentally, are used for the computations. It is well known that the evaluation of physico-chemical parameters is a critical issue when modeling SHS processes (cf. Munir and Anselmi-Tamburini, 1989; Merzhanov, 1993; Varma *et al.*, 1998). In our case, we took advantage of the corresponding values reported by several studies available in the literature, as indicated in Table 10. In particular, the evaluation of the thermal conductivity of our powder mixture was performed by taking into account the model proposed by Luikov *et al.* (1968), which has been recently used also by Bowen and Derby (1993).

Since the ratio between the heat exchanged through the lateral surface of the reacting mixture of conical shape and that one liberated by the reaction in each cross section is proportional to the inverse of the cone radius, the combustion front is forced to stop before reaching the apex, as shown in Figure 19. Here, three time sequences of the combustion front evolution in terms of temperature (a) as well as degree of conversion (b) resulting from the model simulation of the quenching process taking place for system CFQCW are shown. As the reacting mixture is ignited ( $t = 0$  s), the combustion front starts to

propagate and moves towards the apex of the wedge until quenching occurs ( $t = 6$  s).

As it may be seen from Figure 19, a relatively large temperature decay is observed between the reacting mixture and the copper block. This decay is mainly localized at the reacting mixture/copper block interface. Inside the copper block, on the other hand, temperature gradients are relatively smaller and the temperature increases only slightly. This result provided by the two-dimensional model proposed in this work is consistent with the experimental data reported in Figure 20 for the case of 20 % wt of titanium carbide as diluent, where it is seen that while the temperature in the reacting mixture reaches values up to about 3000 °C, the temperature at the outer surface of the copper block remains lower than 70 °C. In addition, the model predicts the presence of unconverted green mixture close to the reacting mixture/copper block interface. This finding is confirmed experimentally by the occurrence of a layer of unreacted powders at that interface, as also observed in previous works (cf. Orrù *et al.*, 1998). Therefore, a one dimensional description of the copper block front quenching technique, as previously developed in the literature (cf. Stepanov and Rogachev, 1992), where the heat transfer inside the block is practically assumed to be at steady state, should be avoided, because it would result in high temperatures at the copper/air interface as well as complete conversion at the reacting mixture/copper block interface.

### **SHS technological applications: ceramic lined pipes.**

Ceramic coatings have acquired a role of considerable importance in a wide variety of technological applications such as electronic devices, optics, chemical processing and corrosion protection. The techniques for producing these coatings are correspondingly diverse, e.g. glazing, screen printing, plasma spraying, spray pyrolysis, sol-gel processing, physical and chemical vapour deposition (Atkinson, 1992). An alternative technique for the preparation of chemical and physical coatings is represented by SHS, as discussed in a recent review article (Grigor'ev and Merzhanov, 1992). By combining SHS with the presence of centrifugal forces, a novel technology, otherwise known as the centrifugal-thermite (CT) process, has been recently developed to produce long ceramic lined pipes (Odawara, 1990, 1992). These can be used for transportation of molten metals or highly corrosive chemical substances, due to their properties such as for example high resistance to corrosion, abrasion and heat. The process, as schematically shown in Figure 21, is based on the occurrence of the SHS thermite reaction between aluminum and iron oxide powders, in presence of specific additives to reduce the violent character of the reaction. The mixture is first distributed over the inside surface of the rotating pipe, and then ignited. Due to the large heat of reaction, the temperature values reached during this process (i.e. about 2500 K) the complete melting of reaction products, i.e. Fe (m.p. 1808 K) and  $Al_2O_3$  (m.p. 2345 K), is obtained. The latter ones are separated because of their different densities under the action of a field of centrifugal forces. A coating constituted by a ceramic layer of alumina is formed in the innermost region of the pipe and an iron layer results between the substrate pipe and the alumina layer.

CT process is influenced by several operating variables, such as the mass ratio of thermite to substrate pipe, the centrifugal acceleration, the thermite powder density, the presence of different additives, the distribution of reactant particle size, etc., whose effect appear not to be studied in a systematic manner (Chandran *et al.*, 1995; Odawara, 1990, 1992; Yin *et al.*, 1993).

For this reason we investigated this process (Orrù *et al.*, 1995; 1996) to gain a deeper understanding of the combined effect of some important operating variables, i.e. mass ratio of thermite mixture to substrate pipe, centrifugal acceleration and additives type and content, in order to identify a suitable monitoring and controlling strategy to obtain a coating with desired microstructure and properties.

The manufacturing process consists first in distributing a uniform layer of the starting mixture blended with acetone, as dispersing agent, into the inner wall of steel pipes (inner diameter of 38 mm, wall thickness of 2 mm and length of 80 mm) to be coated. Drying operations are then performed at room temperature, in order to avoid the formation of cracks, as acetone evaporates. During this step the pipe is rotating with a constant speed of 200 rpm. After drying is completed, the speed is increased to the desired level and ignition is accomplished by using a thermal ignition source, i.e. an oxyacetylene torch. As soon as the ignition is detected, the energy source is turned off. The reaction front then self-propagates rapidly through the reacting mixture, thus reaching the opposite end of the pipe within 2-3 s. After completion of the reaction, the pipe is kept rotating for cooling purposes.

First, we performed a systematic investigation of the effect, upon the stratification and adhesion of the obtained coating, of four important operating variables, i.e. the diluent type and its weight percentage content in the starting mixture (%D), the mass ratio of thermite mixture to outer pipe ( $M_R$ ) and the centrifugal acceleration during the combustion evolution, which is proportional to the square of the rotating speed of the pipe (N). The corresponding operating conditions are summarized in Table 11. The strategy adopted during the systematic study consists in keeping constant three of the operating variables mentioned above, while letting the fourth one to vary within a certain range.

By increasing the diluent ( $\text{SiO}_2$ ) content, smaller amounts of the heat generated by the reaction are available for maintaining products under melting conditions, where centrifugal forces can display their separation effect. In fact, the formation of stratified reaction products may be obtained only if the time needed for separation is much less than the corresponding one for the solidification process. When this condition does not occur, phase separation is hindered and the produced iron results to be highly dispersed into the oxide products.

Conversely, as  $M_R$  increases phase separation is promoted due to the fact that more heat is liberated during the reaction, thus maintaining the products under melting conditions for longer times. With  $M_R > 0.5$  an excessive stratification of the reaction products, resulting in a total separation of the oxide layer from the coating, was found.

Same results are obtained increasing the centrifugal acceleration, N. Moreover, as this operating variable is increased, the porosity of the obtained coating decreases due to volumetric compression of partial gasifying of substances which occurs owing to high temperatures involved as pointed out by Merzhanov and Yuhvid (1990).

Finally, we investigated the influence of the type of diluent on the final coating characteristics, considering also alumina as diluent since, in SHS technology, reaction products are typically used for this purpose (Varma and Lebrat, 1992). By substituting the 50% of the silica content with alumina, although phase separation between the produced iron and oxide products is partially achieved, the bonding of the coating with the substrate pipe becomes worse. This finding is even more evident when totally substituting silica with alumina.

The considerations above lead to the conclusion that, for the set of variables considered, the operating conditions corresponding to  $N = 3500$  rpm,  $M_R = 0.4$  and  $\%D(\text{SiO}_2) = 7$ , appears to be a good compromise between phase separation and adhesion. In particular, a SEM view of a cross section of the coated pipe obtained under these conditions is shown in Figure 22, where it may be seen that the thickness of the iron and the oxide layers is found to be approximately 0.5 mm and 1 mm, respectively.

XRD analysis and WDS investigations, performed on the oxide layer, revealed corundum (Al<sub>2</sub>O<sub>3</sub>) and hercynite (FeAl<sub>2</sub>O<sub>4</sub>), as structural components and iron-aluminosilicates in amorphous form, as mentioned above. Analogous results have been obtained by Odawara (1990, 1992) and Yin *et al.* (1993). It is worth recalling at this point that although hercynite contribute to toughness and thermal shock resistance, it may be attacked under strongly acidic conditions (cf. Odawara, 1992).

As observed from Figure 22, although a satisfactory level of stratification is achieved, the adhesion properties of this coating may be improved. For this, we suggest to select a suitable program of variation of the centrifugal acceleration during the synthesis and the cooling steps of the process. In fact adhesion, i.e. the binding between the metal layer and either the ceramic one or the substrate pipe, depends primarily on centrifugal loading and temperature evolution in time during the coating preparation (Howe, 1993). These variables may be in turn controlled by properly varying the centrifugal acceleration (Merzhanov and Yuxhvid, 1990), i.e. the rotating speed of the pipe, by continuously monitoring the temperature during the synthesis process.

### **SHS environmental applications: treatment and recycling of zinc hydrometallurgical wastes.**

Thermite reactions were also proposed to develop a novel technique for treating and recycling of a highly toxic solid waste from electrolytic zinc plants, i.e. goethite waste (Orrù *et al.*, 1999c), obtained as by-product from electrolytic zinc production process (cf. Cigan *et al.*, 1980). These wastes, which typically contain large amounts of iron oxides, are considered hazardous and toxic according to the environmental protection regulation of European Countries due to the presence of heavy metals like Pb, Cd and Cu as well as As and Zn.

The large production of these wastes (about 750,000 and 90,000 tons/year in Europe and Sardinia Italy, respectively), the high cost of disposal and the increasing difficulty to find suitable disposal locations, clearly provide a demonstration of their environmental impact (cf. Pelino *et al.*, 1994; Pelino *et al.*, 1996a; Pelino *et al.*, 1997).

Currently, a variety of processing options which provide possible solutions to this acute environmental problem are proposed in the literature. These include hydrometallurgical and pyrometallurgical techniques (cf. Pelino *et al.*, 1996a and references therein), which are, to some extent, uneconomic or technically risky. On the other hand glassification, i.e. vitrification of the waste so that hazard components are incorporated into an amorphous glassy structure, is not only an option for environmentally benign disposal but also a promising technique (cf. Ionescu *et al.*, 1997; Pelino *et al.*, 1997; 1996b).

We proposed a technique which consists of blending the goethite waste with suitable amount of reducing agents (aluminum or aluminum and silicon) and ferric oxide, as described in Table 12, according to the stoichiometry of Equation (1), if aluminum is used, or



if aluminum and silicon are both used, where Fe<sub>2</sub>O<sub>3</sub> comes either from the waste or is properly added to the reacting mixture in order to guarantee its ignition and reaction propagation. Acetone was also added, as dispersing agents. Each mixture, once dried in air to totally eliminate acetone, is reacted either as loose powders or in the form of cylindrical pellets, in argon or air at atmospheric pressure, using the experimental set up schematically shown in Figure 2, inset a). In general, regardless of the sample type

and composition mixture, the reaction occurs with the evolution of an opaque gaseous phase. Thus, after reaction completion, the reactor was evacuated by bubbling its gaseous content through suitable washing bottles, whose solution was analyzed by means of ionic chromatography to determine the SO<sub>2</sub> absorbed. In addition, two solid products, called P<sub>1</sub> and P<sub>2</sub>, can be distinguished, being the latter one spread out in powder form towards the reaction chamber walls as a consequence of a probable expulsion occurring during the course of the reaction.

A combustion front was able to propagate through the reacting mixture for all the AlArP samples investigated, i.e. up to a goethite waste content of about 54% while for the AlSArP ones the front self-propagates if the waste percentage is > 45%, as clearly shown in Table 12. This behavior is due to the fact that aluminum is a much stronger reducing agent than silicon, as can be determined thermodynamically (cf. Wang *et al.*, 1993). This aspect is confirmed by the lower levels of maximum combustion temperatures detected when increasing goethite content or using also silicon as reducing agent, and reported in Table 12. It is worth noting that in this latter case, the maximum temperatures measured are close to 1800 K, which is considered the minimum adiabatic temperature required for the feasibility of SHS reactions (cf. Munir and Anselmi Tamburini, 1989; Varma and Lebrat, 1992; Merzhanov, 1995; Hlavacek and Puszynski, 1996; Varma *et al.*, 1998).

However, using only aluminum as dispersing agent, the final products display crystalline character which is, of course, not appropriate when developing a vitrification process. On the other hand, it was clearly shown that only when using Al and Si together as reducing agents, the corresponding XRD spectrum of the product P<sub>1</sub> is consistent with the presence of an amorphous matrix as it may be seen from Figure 23 for the case of AlSArP/a sample. This result is confirmed in Figure 24, where a SEM back scattered micrograph of product P<sub>1</sub> is shown.

It is also interesting to note that when using aluminum and silicon together as reducing agents, the mass ratio between products P<sub>1</sub> and P<sub>2</sub> is greater with respect to the case when only aluminum is employed, as shown in Table 12. This aspect may be related to the fact that, in the latter case, the more violent character of the reaction enhances the expulsion of reactants and products from the reacting mixture. Since the use of silicon together with aluminum allows us to obtain an amorphous product P<sub>1</sub>, where the heavy and toxic species are fixed, the possibility of obtaining a relatively larger amount of product P<sub>1</sub>, with respect to the case when only aluminum is employed, may be considered a result of practical value.

For this reason, for the case of Al and Si used together as reducing agents, cadmium and lead content in products P<sub>1</sub> was determined, as reported in Table 13, by means of a spectrophotometer after dissolution in an aqueous mixture of HF, HClO<sub>4</sub>, and HNO<sub>3</sub>. Leaching test results of the same samples are also reported in Table 13, where the maximum allowable concentration of various species according to the Italian environmental regulations are indicated for sake of comparison. It may be seen that the content of all metals in the eluate are below the maximum allowable concentration for landfill sites which pass specific hydrogeological tests regarding soil permeability. Therefore, in these cases, the concentration of all hazardous species considered in the eluate falls well within the prescribed environmental restrictions. It is worth noting that the maximum allowable concentrations reported in Table 13 are, to our knowledge, much more restrictive with respect to those ones considered in other countries.

Since same results were obtained reacting samples with Al and Si together as dispersing agent under air atmosphere, a treatment process of the goethite waste may be proposed at industrial level. A schematic

representation of this process is reported in Figure 25. The goethite waste can be first mixed with hematite and reducing agents, i.e. aluminum and silicon, under appropriate mass ratios. It is important to note that mixing with acetone should be certainly avoided for larger scale use. Then, the obtained mixtures can be reacted inside suitable reaction chambers, whose technology is already available for the synthesis of materials by SHS (cf. Merzhanov, 1995 and references therein). The resulting product  $P_1$  may be disposed in landfills. The possibility of recycling such product in the glass-ceramic industry is being currently investigated. Product  $P_2$  on the other hand may be recycled directly within the zinc production plant, i.e. the sphalerite roasting unit, due to its composition (Enirisorse, 1996). The produced gas may be treated within the same production plant, where the  $SO_2$  abatement unit is already operating.

It is worth noting that an economic evaluation of the large-scale process is currently being performed. Although relatively large ratios of added (Al/Si) and  $Fe_2O_3$  to waste have to be used, as it may be seen from Table 12, the objective is to take advantage of aluminum, silicon and ferric oxide scraps which are readily available on the market and relatively inexpensive. In addition, it is expected that the economic evaluation of the entire process depends also upon the possibility of recycling product  $P_2$  in the roasting plant, since this option might determine a mineral input saving.

### **SHS environmental applications: the degradation of chloro-organic compounds.**

Another environmental application of SHS reactions, i.e. degradation of highly toxic chloro-organic compounds, was successfully investigated (Cao *et al.*, 1999). It is worth mentioning that powder mixtures of chloro-organics and reactive substrates, i.e. Ca and Mg and their oxides, were treated by BM thus obtaining a complete degradation of the organic compounds under inert or hydrogen atmospheres (cf. Australian patent Application PL6474, 1992; Rowlands *et al.*, 1994; Loiselle *et al.*, 1997). By increasing the milling intensity beyond a well defined impact energy threshold, an explosive-like reaction was observed, leading to gaseous hydrogen, graphite and calcium chloride salts as end products (cf. Mulas *et al.*, 1997). The degradation process can be carried out in a confined and strictly controlled environment, i.e. in absence of oxygen. Thus, the BM methodology is highly attractive because it prevents the formation of hazardous oxidised congeners.

However, there are some inherent limitations to BM practical exploitation. A problem is represented by the scaling up of a laboratory milling reactor by several orders of magnitude to a size of interest to industry. The difficulties seem mainly linked to the development of a leak-proof technology owing to the dynamic operating conditions of the grinding tools. In addition, the complete breakdown of the organic molecules is achieved after relatively long milling times, usually of the order of hours, requiring a conspicuous consumption of energy. These shortcomings and other related problems point out the need for alternative activation methods to the mechanochemical route.

Thus, bearing in mind the strongly exothermic characteristics of the reactions involved, the possibility of triggering dehalogenation processes by conventional ignition methods was verified, and a comparison between SHS and BM results obtained from parallel experiments with the two different techniques has been carried out for the first time in the literature. Note that the intensification of diffusion reaction by milling to a spontaneous propagation stage, referred to as SHS mechanochemistry (SHSM) (cf. Merzhanov, 1995b), is a relatively new topic in the field.

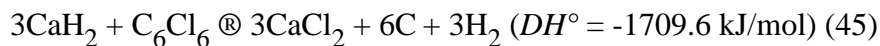
The reaction between hexachlorobenzene and calcium hydride as prototype system is considered in this



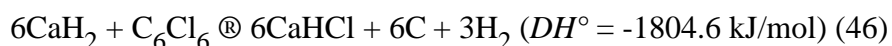
review paper. The schematic diagram of the SHS setup used is depicted in Figure 2 inset a), while BM experiments were carried out with a commercially available mill. Starting mixtures were prepared blending commercial powders of calcium hydride and hexachlorobenzene at different molar ratios ( $\text{CaH}_2/\text{C}_6\text{Cl}_6 = 3, 4, 6, 9, 12, 15$  and  $18$ ), and pressed into cylindrical pellet up to a green density ranging from  $2.7$  to  $3.2 \text{ g/cm}^3$ , or used as loose powders, for SHS or BM experiments, respectively. In both cases an inert environment, i.e. argon at  $1 \text{ atm}$ , was provided. Details of experimental set up and procedure are reported elsewhere (cf. Cao *et al.*, 1999) for sake of brevity.

In Figure 26 it may be seen that high-temperature pyrolysis of hexachlorobenzene can be carried out under thermally-ignited self-sustaining regimes. Regardless of the mixture composition, the reaction evolution occurs with release of a large amount of gaseous products and a wave velocity in the range  $0.5$ – $1.0 \text{ cm/s}$ , i.e. well within the typical range found in the combustion synthesis of inorganic materials ( $0.1$ – $25 \text{ cm/s}$ ) (cf. Munir and Anselmi-Tamburini, 1989; Merzhanov, 1994; Varma *et al.*, 1998). Due to the violent evolution of gaseous products, amounts of powders were spread out in the reaction chamber, so that the mass of the residual pellet core,  $P_1$  can be distinguished from the total mass of the original pellet,  $P_0$ . XRD analysis of combusted powders was carried out, while gas products were sampled from the reactors head space through leak-proof valves and analysed by a gas chromatograph equipped with a flame ionization detector. To control the presence of residual hexachlorobenzene or possible organic compounds the reacted powders were treated in *n*-pentane and analysed by a gas chromatograph and a Mass Spectrometer.

A precise  $\text{CaH}_2$ - $\text{C}_6\text{Cl}_6$  stoichiometry is required for the complete reduction of organic chlorine. Assuming a straight decomposition route,



the  $\text{CaH}_2/\text{C}_6\text{Cl}_6$  molar ratio remains set at 3. By increasing the  $\text{CaH}_2$  content above a molar ratio of 6, the formation of the mixed hydride chloride is favoured according to the following transformation path



As expected from these high exothermic reactions, a self sustaining behavior was observed in the whole interval of composition tested, extending from a molar ratio of 3 to 18.

Although safety problems seem of minor concern in the case of SHS experiments, the progressive explosive character of the reaction pose some restrictions, when moving towards higher  $\text{C}_6\text{Cl}_6$  contents. Due to the violent evolution of gaseous products, growing amounts of powder were spread out in the reaction chamber, as the reactant molar ratio increases.

X-ray analysis of the solid end-products carried out in parallel at the end of both SHS and SHSM processes, are shown in Figure 27. As can be seen, the same combustion products are obtained for a reactant mixture with a molar ratio equal to 12. In Figure 27 we also report the pattern of the SHS combusted powders after chemical passivation under an argon-air stream in order to expose the final powders to X-ray analysis without resorting special conditions.

From Table 14 it is seen that we did not find residual chlorinated organic compounds in the solid phase.

In fact, their content is at the ppm level, as it may be seen in Table 14 where the GC/MS results of the solid-phase are reported.

The analysis of the gas phase sampled at the end of the self propagating degradation revealed the presence of hydrogen, carbon monoxide, methane, benzene, toluene and chloro-benzene, whose content is reported in Table 15 for the case of a reactants molar ratio equal to 9. Note that the solid end products and the gas composition above is representative also of the other mixtures studied in this work. It should be noted that the methodology proposed here has been successfully applied also to the destruction of a commercial herbicide known as Dichlorprop (cf. Cocco *et al.*, 1999) and thus it may be regarded as an innovative disposal method for chlorinated waste compounds.

**Acknowledgements:**

Most of the results reported in this review paper have been obtained in the framework of scientific collaborations with Professors G. Cocco, Z. A. Munir and A. Varma and Drs. S. L. Kharatian and H. H. Nersisyan.

**Nomenclature**

a moles of low melting reactant, A per mole of nonmelting reactant, B in the initial mixture

b moles of inert diluent, P per mole of nonmelting reactant, B in the initial mixture

Bi Biot number,

concentration of gaseous reactant at the interface between the ash layer and the unreacted core,

concentration of low melting reactant, A in the surroundings of the nonmelting particle,

C<sub>p</sub> heat capacity,

Da Damkholer number,

pre-exponential effective diffusivity of the melting reactant, A,

average particle diameter of the nonmelting reactant, B at any time t,

,  activation energies,

g(t) quantity defined in equation (43)

$h$  natural convection heat transfer coefficient,

$H_0$  wedge height, m

$H_t$  copper block height, m

$k$  thermal conductivity,

$k_g$  gas-film mass transfer coefficient,

adsorption equilibrium constant for gaseous reactant,

$k_0$  frequency factor,  $s^{-1}$

$k_{i0}$  frequency factor for gas-solid SHS reactions, units depend upon kinetics

$m$  empirical parameter

$M$  molecular weight,

$M_R$  mass ratio of thermite mixture to outer pipe

$n$  reaction order

unit vector normal to conical surface, m

$N$  rotational speed, rpm

$P$  pressure, atm

$p$  ignition energy flux,

$q$  mole of diluent per mole of nonmelting component in the initial mixture

$r$  radial coordinate, m

$R_i$  radius of unreacted core of the solid particle, m

$R_t$  copper block radius, m

$R_0$  wedge initial radius, or unreacted solid particle radius, m

T temperature, K

t time, s

$t_q$  ignition time, s

velocity of the combustion front in solid-solid systems,

w velocity of the combustion front in gas-solid systems,

z longitudinal coordinate, m

### **Greek letters**

$\alpha$  wedge half angle, deg

b ratio between the thickness of intermetallide complex, and the initial particle diameter of the nonmelting reactant B

$\epsilon$  mixture void fraction